Delft University of Technology

Realisation of plasma synthetic jet array with a novel sequential discharge

Zong, Haohua; Kotsonis, Marios

Citation (APA)
Zong, H., & Kotsonis, M. (2017). Realisation of plasma synthetic jet array with a novel sequential discharge. *Sensors and Actuators A: Physical: an international journal devoted to research and development of physical and chemical transducers*, *266*, 314-317. https://doi.org/10.1016/j.sna.2017.09.027

Important note
To cite this publication, please use the final published version (if applicable).
Please check the document version above.

Realisation of Plasma Synthetic Jet Array with a Novel Sequential Discharge

Haohua Zong* and Marios Kotsonis

Faculty of Aerospace Engineering, Delft University of Technology, Delft 2629 HS, Netherlands

Abstract: The Plasma Synthetic Jet Actuator (PSJA) is a zero-net mass flow actuator, capable of producing supersonic pulsed jets at high frequency (>5kHz). Successful application of PSJA to active flow control necessitates the removal of two obstacles, namely, low energy conversion efficiency and small jet affected length. A novel sequential discharge scheme employing a simple architecture is proposed to feed a PSJA array of multiple actuators. Phase-locked Particle Imaging Velocimetry (PIV) and electrical measurements are exploited to quantify the performance of the PSJA array. The jet impulse and jet mechanical energy of the PSJA array first improves and then drops, when the actuator number ranges from 1 to 6. Compared to that of single actuator, the discharge efficiency of PSJA array at an actuator number of 4 is increased by 10%, and the electro-mechanical energy is augmented by 340%. Additionally, the jet affected length is extended from the order of 10 mm to the order 100 mm.

Synthetic jets (SJ), also referred to as zero-net mass flow jets, receive renewed interest from the active flow control community due to their application potential in drag reduction, lift augmentation, noise mitigation and boundary layer transition control (Glezer & Amitay 2002, Mohseni & Mittal 2014). Compared with other varieties of SJ actuators including piezoelectric-type and piston-type actuators, the plasma synthetic jet actuator (PSJA) is unique in featuring generation of high-velocity (>5kHz) high-frequency (>300 m/s) pulsed jets in a simple and compact structure (Narayanaswamy, Raja & Clemens 2010). Notwithstanding the jet intensity, the PSJA exhibits two notable limitations, which need to be overcome for industrial applications. These are the low energy conversion efficiency (O(0.1%)) and small jet-affected length (O(10 mm)) (Zong et al. 2016).

In large-scale applications such as airfoil separation control, tens of actuators arranged in an array may be needed (Alexander et al. 2016). As such, the issue of how to effectively feed the PSJA array (namely multiple-channel arc discharge) stands out. The preliminary scheme of one power supply per actuator adopted initially in laboratory tests is not feasible in practice due to the assosciated complexity and weight penalty (Narayanaswamy, Raja & Clemens 2012). Zhang et al. (2017) proposed a sequential breakdown scheme and demonstrated simultaneous operation of up to 13 actuators with one power supply system. However, under this concept, the extension of the array by one actuator is accompanied by the addition of an extra resistor and a high-voltage capacitor to the power supply system, resulting in a complex structure and considerable space and weight penalty. In this study, a novel sequential discharge scheme is proposed to feed the PSJA array. No addition of electrical components is needed to incorporate an extra actuator into the array. The influence of the actuator number on the overall performance of PSJA array is investigated in detail with electrical and phase-locked PIV measurements.

As shown in Figure 1, a PSJA array embedded with six ceramic actuators is designed and positioned within a nylon support base. Both the ceramic cube (outer dimension: 15*15*15 mm^3) and the ceramic cap are made of MACOR ceramic. Each ceramic cube houses a cylindrical cavity (diameter: 10 mm, height: 10 mm), accommodating the discharge. Two tungsten needles are inserted into the cavity through two opposite sides of the ceramic cube, serving as anode and cathode respectively. The electrode distance can be adjusted by the electrode holder and fixed at 2 mm for all the actuators in the current study. Additionally, a thin capillary tube is inserted centrally through the bottom of the ceramic cube, to accommodate provision of PIV seeding in the cavity. The ceramic cap provides an airtight closure of the cavities towards forming six individual actuators. Six round orifices in a diameter (D) of 1.5 mm and spacing of 15 mm are drilled in the cap, aligned with the center of each actuator cavity. A coordinate system is established in the center of the first exit orifice as shown in Figure 1.
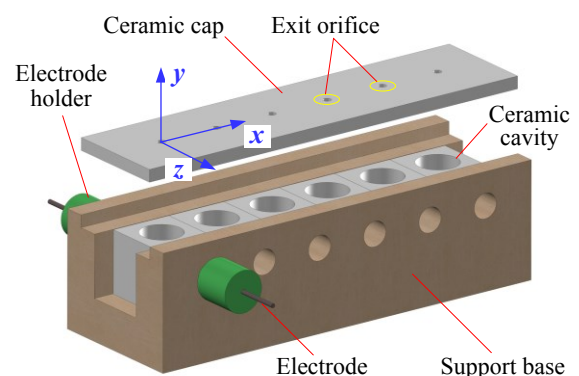

Figure 1. Structure of PSJA array

The six actuators in the PSJA array are connected in series, and fed by a sequential discharge (trigger discharge-capacitive discharge) power supply as shown in Figure 2. By appropriate connection of the cables,

four cases with different actuator numbers (N_d=1, 2, 4 and 6) are tested.

The charge circuit consists of a DC power supply (voltage: 2 kV, maximum power: 2 kW), a current-limiting resistor R1 (resistance: 1 kΩ, power: 100 W) and a high-voltage capacitor C1 (capacitance: 1 μF). The trigger pulses (peak voltage: 20 kV, width: 100 μs) used to establish discharge channels are produced by a high-voltage amplifier (Trek Model, 20/20C). Two high-voltage diodes (D1 and D2, withstanding voltage>30kV) are added to isolate the charge and the trigger circuits. After the ignition of all the discharge channels, the energy stored in C1 is released rapidly to the actuator cavities, and strong pulsed jets are created through the orifices. Subsequently, the capacitor C1 is recharged, in preparation for the next pulse.
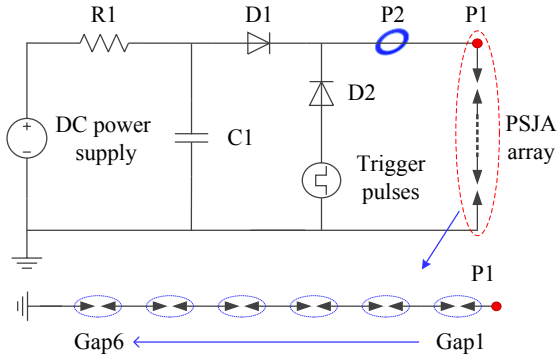

Figure 2. Power supply system. The red dot (P1) and the blue ring (P2) indicate the voltage and the current measurement station, respectively. The PSJA array is shown as six gaps. The numbering sequence of gap and actuator (from anode to cathode) is consistent throughout the paper.
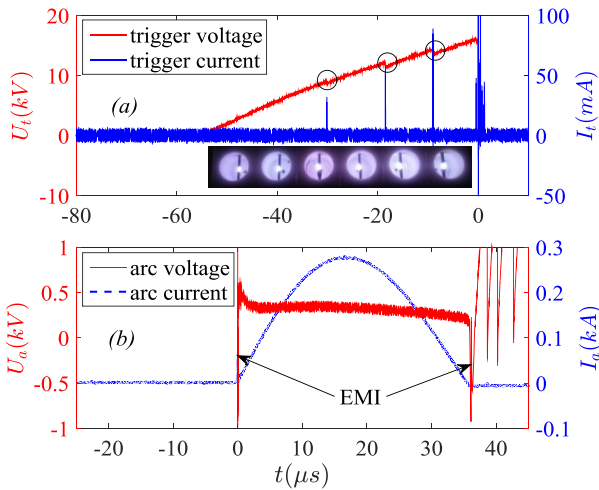

Figure 3. Discharge waveforms for the PSJA array with six actuators. (a) Trigger discharge and (b) pulsed arc discharge. The red circles indicate several abrupt drops of trigger voltage. Abnormal peaks caused by electromagnetic interference (EMI) are indicated in the trace of arc voltage.

Discharge waveforms at a capacitor voltage (U_c) of 2 kV are measured by a high-voltage probe (Tektronix, P6015A) and a current monitor (Pearson, Model 325), and recorded by an oscilloscope (Tektronix, TDS 3054C). Measurement stations are indicated in Figure 2. Traces of the trigger voltage (U_t), arc discharge voltage (U_a) and discharge current (I_d) for the six-actuator array,

are shown in Figure 3. The picture of trigger discharge attached in Figure 3 (a) was taken by a Canon camera (EOS 750D, exposure time: 1/30 s) at a trigger frequency of 200 Hz.

The trigger voltage increases steadily to 15.5 kV until the occurrence of final breakdown. Six bright arcs are created in the gaps afterwards, indicating a fully linked discharge channel. Three small yet abrupt drops are observed in the rising edge of U_t, which can be attributed to the sudden change of load characteristics, namely the sequential breakdown events. As a consequence, there exists a significant time delay (30 μs) between the breakdown of the first and the last gap. This differs largely from the discharge reported in Zhang et al. (2017), where a time delay of less than 1 μs is recorded. During the discharge, the arc voltage remains approximately at 300 V and experiences considerable electromagnetic interference during the ignition and quench phase. The integral of U_a and I_d with time (t) defines the discharge energy (E_d). The ratio of discharge energy to capacitor energy (E_c) further gives the discharge efficiency (η_d),

$$\begin{cases} E_d = \int_0^{T_d} U_a I_d \cdot dt \\ \eta_d = \dfrac{E_d}{C_0 U_c^{\,2}/2} \end{cases} \quad (1)$$

where, T_d and C_0 are the discharge duration and the capacitance of capacitor C1. For capacitive discharge, the arc is typically modeled as a constant resistor and the equivalent resistance (R_{arc}) of the whole discharge channel can be determined by the following relation,

$$R_{arc} = \frac{E_d}{\int_0^{T_d} I_d^{\,2} \cdot dt} \quad (2)$$

Table 1. Discharge parameters with different actuator numbers

N_a	U_b(kV)	R_{arc} (Ω)	E_d (mJ)	η_d (%)
1	7.2	0.68	1109	55.4
2	8.6	0.78	1213	60.7
4	12.3	0.93	1305	65.2
6	15.7	1.04	1316	65.8

For different actuator numbers, the aforementioned discharge parameters are listed in Table 1. All the data are statistically averaged values computed from 5 uncorrelated pulse runs. As expected, the breakdown voltage increases with gap number. Comparing the highlighted voltage ratings in Figure 3 (8.9 kV, 12.4 kV, 14.6 kV and 15.5 kV) to the breakdown voltages of different gap numbers listed in Table 1, the sequential ignition phenomenon of electrode gaps can be confirmed. The discharge energy, as well as the equivalent arc resistance increases monotonically with actuator number, as a result of the elongation of discharge channel. Additionally, the discharge efficiency is improved moderately from 55.4 % to 65.8 %.
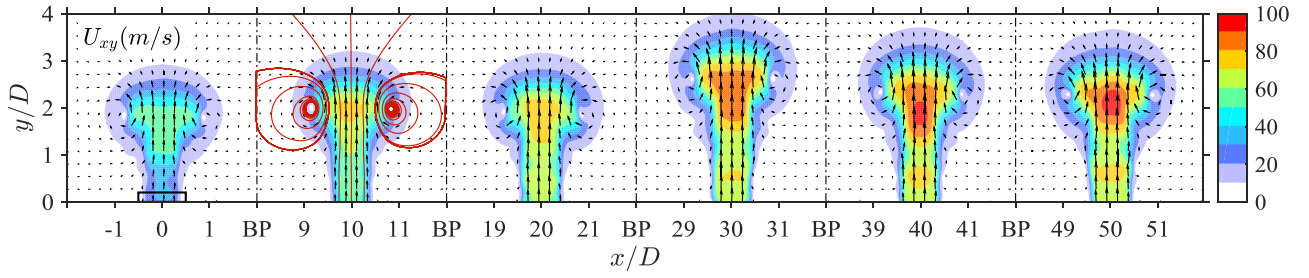
Figure 4. Phase-averaged flow field at t=200 μs. Note that breakpoints (denoted as BP) are used in the x-axis to condense the display range. The solid black rectangle just above the exit in the first plot indicates the interrogation window used to get phase-averaged exit velocity. The red lines in the second plot are streamlines.

A phase-locked Particle Image Velocimetry (PIV) system is adopted to measure the jet-induced flow field in the xy-plane. Two 16-MPx camera (Lavision Pro LX) are placed side by side to form a combined field view of approximately 95×35 mm^2, which is sufficient to cover the induced flow of six actuators. The laser beam emitted from a dual-head Nd:YAG laser (Quantel, EverGreen) is shaped into a thin sheet (thickness: ~0.5 mm), passing strictly through the exit orifice center. The camera lenses, programmable time unit (PTU), seeding system and signal synchronization scheme are described in Zong & Kotsonis (2016a). For each phase of the four test cases (N_a=1, 2, 4, 6), 200 image pairs are recorded at sampling rate of 0.75 Hz to get phase-averaged flow fields. Davis 8.3 is used to acquire and process image pairs. A spatial resolution of 16 vectors/mm is reached with a final interrogation window size of 24×24 pixels. and an overlapping ratio of 75%.

For the PSJA array with six actuators, the phase-averaged flow field at a time delay of t=200 μs in respect to the discharge ignition is shown in Figure 4. U_{xy} denotes the Euclidean sum of the in-plane velocity components (U_x and U_x). The flow fields produced by individual actuators present a similar topological arrangement. An auspicious vortex ring lies in the jet front. In the center of this front vortex ring, a high-velocity region is observed due to the self-induced effect. Apart from this similarity, a considerable difference exists regarding the individual jet intensity. The peak jet velocity for the 4th actuator reaches approximately 100 m/s, in contrast with 70 m/s for the 1st actuator. From the perspective of jet height, the highest and the lowest differ by 2 mm (25% relative difference).

To further visualize the pertinent differences between actuators, the spatially-averaged exit velocity (U_{ex}) is monitored within a rectangle window (width: 1.5 mm, height: 0.2 mm) just above the orifice exit, as indicated in Figure 4. Variations of U_{ex} in one period for the six jets are displayed in Figure 5. The earlier ignited actuators demonstrate a lower peak jet velocity and shorter jet duration, namely weaker pulsed jet. Based on the phase-averaged exit velocity curves in Figure 5, three crucial integral parameters pertaining to the single jet pulse including the expelled gas mass (m_e), jet impulse (I_p) and jet mechanical energy (E_m), can be estimated using the simplified model in Zong & Kotsonis (2016b). For the array with six actuators, the comparison of I_p and E_m between individual jets is shown in Figure 6.
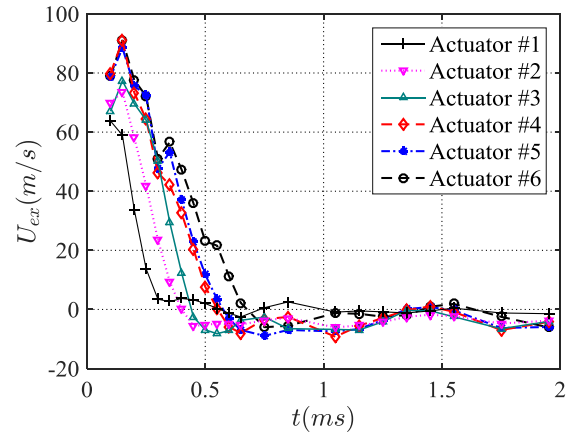

Figure 5. Comparison of exit velocity evolution within one period. The numbering of actuator is consistent with Figure 2.
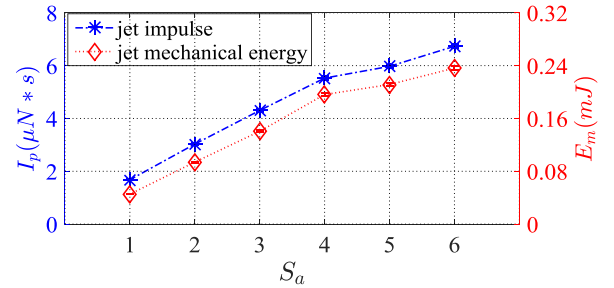

Figure 6. Intensity comparison between individual jets for the six-actuator array. S_a represents the numbering of the actuator.

The strongly monotonic variation (four times increase in I_p and five times increase in E_m) excludes the possibility of ascribing the jet intensity distinction to systematic errors, such as discharge energy fluctuation caused by the minor difference in electrode distance (±0.1 mm). Based on the observations, the distinction in jet intensity can be related to the different heating efficiency incurred by the sequential ignition scheme. Specifically, the heating efficiency of the capacitive discharge is closely related to the local atmospheric parameters in the electrode gaps. For the early ignited electrode gaps, the gas in the cavity is gradually thermalized, leading to a declined density prior to the ignition of the next capacitive discharge. In a low-density environment, a significant drop of heating efficiency in the capacitive discharge is observed by Smy et al. (1983). This deterioration in heating

efficiency directly results in the declined jet intensity of early ignited actuators.

The overall performance of an array is defined by the summation of individual actuator's performance. Specifically,

$$X_A = \sum_{i=1}^{N_a} X_i \qquad (3)$$

where, X_i can be either of the three metrics (m_e, I_p and E_m); X_A corresponds to the respective three performance metrics pertaining to the entire actuator array (m_{Ae}, I_{Ap} and E_{Am}) and N_a is the total number of actuators in the array. m_{Ae} is further normalized by the initial gas mass in one actuator cavity, resulting in a nondimensional mass, $\bar{m}_{Ae} = m_{Ae} / (\rho_0 V_{ca})$, where ρ_0 is ambient density and V_{ca} is cavity volume.

The electro-mechanical efficiency of PSJA array (η_m) is defined as the ratio of total jet mechanical energy to arc discharge energy, E_{Am}/E_d. For the considered PSJA array with different N_a, the abovementioned metrics are listed in Table 2 and further displayed in Figure 7.

Table 2 Jet performance parameters of PSJA array

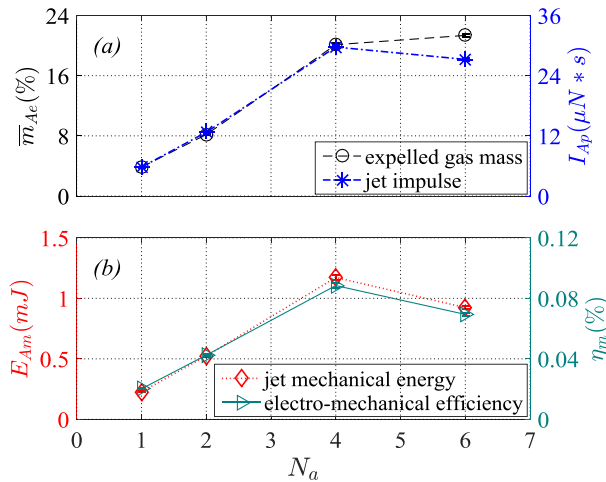| N_a	$\bar{m}_{Ae}$ (%)	I_{Ap} (μN·s)	E_{Am} (mJ)	η_m (%)
1	3.8	5.8	0.23	0.020
2	8.2	12.7	0.52	0.042
4	20.1	29.7	1.17	0.088
6	21.4	27.2	0.92	0.069

Figure 7. Overall performance parameters of PSJA array with different actuator numbers.

The demonstrated trends for all the performance metrics follow similar behavior. When the actuator number increases from 1 to 4, $\bar{m}_{Ae}$, I_{Ap} and E_{Am} increase almost linearly. Further examination shows that the averaged jet intensity parameter (X_A/N_a) also increase slightly. This is largely beyond the authors' expectation, as the discharge energy distributed to single actuator (E_d/N_a) is actually decreasing when new actuators are added to the array. Further experiments are needed to clarify the source of this effect.

When the actuator number reaches 6, a drop is experienced in the jet impulse and jet mechanical energy, whereas the nondimensional expelled gas mass

exhibits a mild increase from 20.1% to 21.4%. This severely deteriorated performance of the PSJA array is attributed to the declined electro-mechanical efficiency of individual actuators, which scales with the nondimensional energy deposition (for the investigated case, E_d/N_a). Variation of the electromechanical efficiency loosely follows the jet mechanical energy, and the peak value reaches 0.088 %, which is less than that of a similar single-cavity case reported in Zong & Kotsonis (2016b) (Case 2, 0.144%). The distinction is attributed to the different electrode configuration (three-electrode configuration in Zong & Kotsonis 2016b as opposed to a two electrode configuration in the present study), whose dramatic influence on the efficiency of single actuator has been demonstrated in Zong et al. (2015).

In conclusion, a novel sequential discharge scheme has been proposed to feed the PSJA array, requiring no extra electrical components for the addition of new actuators to the array. With constant capacitor energy, the PSJA array performs optimally at an actuator number of 4 for the tested settings. However the performance is reduced for a higher number of actuators. Comparing the performance of the PSJA array to that of a single actuator, the discharge efficiency is improved from 50% to 60%, and the electro-mechanical energy is augmented by 340%. Another significant contribution is the jet affected scale, which is increased from $O(10)$ mm to $O(100)$ mm, a noteworthy step towards industrial application.

References

Alexander, M. G., Harris, F. K., Spoor, M., Boyland, S. R., Farrell, T., & Raines, D. (2016). Active Flow Control (AFC) and Insect Accretion and Mitigation (IAM) System Design and Integration on the Boeing 757 ecoDemonstrator. In 16th AIAA Aviation Technology, Integration, and Operations Conference (p. 3746).

Glezer, A., & Amitay, M. (2002). Synthetic jets. Annual review of fluid mechanics, 34(1), 503-529.

Mohseni, K., & Mittal, R. (Eds.). (2014). Synthetic Jets: Fundamentals and Applications. CRC Press.

Narayanaswamy, V., Raja, L. L., & Clemens, N. T. (2010). Characterization of a high-frequency pulsed-plasma jet actuator for supersonic flow control. AIAA journal, 48(2), 297-305.

Narayanaswamy, V., Raja, L. L., & Clemens, N. T. (2012). Control of unsteadiness of a shock wave/turbulent boundary layer interaction by using a pulsed-plasma-jet actuator. Physics of Fluids, 24(7), 076101.

Smy, P. R., Clements, R. M., Dale, J. D., Simeoni, D., & Topham, D. R. (1983). Efficiency and erosion characteristics of plasma jet igniters. Journal of Physics D: Applied Physics, 16(5), 783.

Zhang, Z., Wu, Y., Jia, M., Song, H., Sun, Z., Zong, H., & Li, Y. (2017). The multichannel discharge plasma synthetic jet actuator. Sensors and Actuators A: Physical, 253, 112-117.

Zong, H. H., Wu, Y., Jia, M., Song, H. M., Liang, H., Li, Y. H., & Zhang, Z. B. (2015). Influence of geometrical parameters on performance of plasma synthetic jet actuator. Journal of Physics D: Applied Physics, 49(2), 025504.

Zong, H., Wu, Y., Song, H., & Jia, M. (2016). Efficiency Characteristic of Plasma Synthetic Jet Actuator Driven by Pulsed Direct-Current Discharge. AIAA Journal, 3409-3420.

Zong, H., & Kotsonis, M. (2016a). Characterisation of plasma synthetic jet actuators in quiescent flow. Journal of Physics D: Applied Physics, 49(33), 335202.

Zong, H., & Kotsonis, M. (2016b). Electro-mechanical efficiency of plasma synthetic jet actuator driven by capacitive discharge. Journal of Physics D: Applied Physics, 49(45), 455201.